Phys. Status Solidi B **250**, No. 1, 77–85 (2013) / **DOI** 10.1002/pssb.201248386

physica status solidi b
www.pss-b.com
basic solid state physics

Intrinsic uncertainty on *ab initio* phase diagram and compound formation energy calculations: BCC Mo–Fe as a test case

Ney Sodré[1], Joelson Cott Garcia[2], Lucy Vitoria Credidio Assali[1], Pablo Guillermo Gonzales-Ormeño[3], Peter Blaha[4], Helena Maria Petrilli[1], and Cláudio Geraldo Schön[*,5]

[1] Departamento de Física dos Materiais e Mecânica, Instituto de Fìsica da Universidade de São Paulo, CP 66318, CEP 05315-970 São Paulo-SP, Brazil
[2] Laboratório de Microeletronica do Departamento de Engenharia de Sistemas Eletrônicos, Escola Politécnica, Universidade de São Paulo, CP 61548, CEP 05424-970 São Paulo-SP, Brazil
[3] Universidad Nacional Tecnológica del Cono Sur de Lima, Sector 3, Grupo 1A 03, Cercado, Villa El Salvador, Lima, Peru
[4] Institut für Materialchemie, Technische Universität Wien, Getreidemarkt 9/165-TC, 1060 Wien, Austria
[5] Computational Materials Science Laboratory, Department of Metallurgical and Materials Engineering, Escola Politécnica da Universidade de São Paulo, Av. Prof. Mello Moraes, 2463, CEP 05508-900 São Paulo-SP, Brazil

Received 23 April 2012, revised 8 August 2012, accepted 21 August 2012
Published online 19 September 2012

Keywords cluster variation method, density functional theory, iron alloys, metastability, miscibility gap, Mo–Fe system

* Corresponding author: e-mail schoen@usp.br, Phone: +55-11-30915726, Fax: +55-11-30915243

Ab initio electronic structure calculations, within the Kohn–Sham scheme of the density functional theory, are often considered reliable and a powerful tool to provide ground state information on intermetallic compounds. More recently, it has been used in multi-scale intermetallic phase diagram calculations with particular importance when experimental data is lacking. In spite of this recent success, they rely on basic choices of the computational solution of the complicated quantum mechanical problem. Therefore, the calculated phase diagrams may depend on these choices. Here, we concentrate on the influence of some methodological aspects of the *ab initio* calculations on the resulting phase diagram, for a given statistical mechanics approach. We use the Full Potential-Linear Augmented Plane Wave and the Projector Augmented Wave Methods to perform electronic structure calculations combined with the cluster variation method in the irregular tetrahedron approximation to calculate the BCC Mo–Fe phase diagram. It is shown that all calculated phase diagrams present similar qualitative features (an asymmetric miscibility gap), but quantitative variations are found depending on some of the basic assumptions adopted for the electronic structure calculations. Based on these results, a "natural" accuracy of the order of $\pm$ 1 kJ mol^{-1} can be estimated for *ab initio* compound formation energies.

1 Introduction The large success achieved by *ab initio* electronic structure methods, in the framework of the Kohn–Sham (K–S) scheme of the Density Functional Theory (DFT) (see Ref. [1] and references therein) has brought a quality jump into many related research fields, since it turned into reality the dreamed promise of Quantum Mechanics to explain macroscopic properties from atomic constituents and spatial arrangements [2]. The impulse in this area is also due to the development of fast computers, which nowadays allows calculations of large and complicated systems. The ground state electronic structure of simple metallic alloys can usually be well described and many measurable quantities, which previously would be roughly reproduced, can now be very precisely predicted. More recently, with the attention driven to multi-scale modeling, a new research community has grown, which uses *ab initio* calculations together with thermodynamic modeling to obtain intermetallic phase diagrams.

Together with the benefit brought by the introduction of state of the art *ab initio* calculations and of user-friendly computer packages, the impulse of this area has introduced many new researchers, non-experts, into the field. One of us has recently discussed [6] some fundamental aspects of the charge density calculations, which are well known for the

experienced researcher, but not so much to newcomers into the field,using a test quantity [6–12] which depends on fine details of the charge density near the nucleus.

On the other hand, the calculation of intermetallic phase diagrams uses as input from the *ab initio* methods the total energy and, to our knowledge, little attention has been given to the influence of some methodological approximations inherent to these electronic structure calculations. Therefore, the discussion has been mainly driven to truncation aspects of the statistical mechanics approach and convergence of the basis set [13].

The Full Potential-Linear Augmented Plane Wave (FP-LAPW) Method [3] has been applied to study many different systems and properties in the last 20 years. It has been implemented into many different computer codes as, for example, the WIEN2k code [3], a user friendly computer package. Another approach which has been introduced into different computer packages as, for example, the ''Vienna *ab initio* simulation package'' (VASP) [5] code, and became a powerful and efficient tool to obtain total energies, even in intermetallic systems, is the PAW method [4]. Here, we investigate the influence on the resulting phase diagram of some methodological approximations in the *ab initio* calculations. We use the FP-LAPW as embodied into the WIEN2k package [3] and the VASP code [5], to perform electronic structure calculations combined with the Cluster Variation Method (CVM) [14] in the irregular tetrahedron (IT) approximation to calculate the BCC Mo–Fe phase diagrams. The procedure adopted in the present work is similar to the one used by some of the present authors in the calculation of the BCC Al–Mo system [15] and of the BCC Fe–Al system [16, 17]. In both cases (as in the present work), we chose to restrain the approximation to a low level (the IT approximation of the CVM) instead of seeking for the convergence of the Cluster Expansion, as suggested by van de Walle and Ceder [13]. By limiting the number of energy parameters entering into the model, a better appreciation of the effects we desire to study is allowed, while still being able to provide useful information on the qualitative features of the phase diagrams.

2 Methodology The procedure used for the Mo–Fe phase diagram calculation is based on the so-called cluster expansion method [18]. In this approach, the total energies at the ground state ($T = 0$ K) of a set of stoichiometric ordered compounds (which are related to a common disordered lattice) are calculated in the K–S scheme of the DFT. This set forms a basis for the truncated expansion of the internal energy of the lattice at all temperatures and compositions, which are then used as input in a statistical mechanics method to calculate the phase diagram.

The set used in the present work is formed by the A2 Mo, A2 Fe, $D0_3$ $MoFe_3$, $D0_3$ Mo_3Fe, B2 MoFe, and B32 MoFe compounds, which is rather limited in comparison, for example, with the one used by Blum and Zunger [19] to investigate the bcc Mo–Ta system (52 compounds). The basis set is kept limited here on purpose since only a simplified thermodynamic description of the system based on the IT approximation of the CVM is targeted. The adopted ground states are highly symmetrical, such that no internal relaxation parameters are needed, and the compounds were optimized only through their lattice parameters. Other less symmetric ground states could, perhaps, be more stable than the ones adopted here, but they are not included in the present calculation since this would go beyond the scope of the chosen approximation.

The total energies of the ordered compounds have been initially calculated using the WIEN2k code [3]. This allows to test the effect of three groups of approximations used in the calculation of the electronic structures, which are:

a) the choice of basis for the expansion of the wave function,
b) the choice of the exchange-correlation part of the electron–electron potential, and
c) the consideration of relativistic effects and spin-orbit coupling.

The first set of calculations, denoted here by ''FPLAPW + LSDA'' was performed with the traditional basis used in the FP-LAPW method, which is formed by orbital-like wave functions inside the spheres and plane waves in the interstitial region. The exchange-correlation effects where considered using the simplest approximation within the DFT, where only the local electronic (spin) density is considered (the so-called Local Spin Density Approximation, LSDA) [20]. Relativistic corrections are applied only in a simplified way, using a scalar-relativistic implementation of the algorithm [21].

The second set, named ''FPLAPW + GGA'' uses the same basis as the previous one, but now the exchange-correlation effects are calculated using the so-called ''Generalized Gradient Approximation'' (GGA). In the present work, the implementation suggested by Perdew, Burke, and Ernzernhof (PBE) has been used [22]. As in the previous case, only scalar-relativistic corrections are applied to this set of calculation.

The third set, named ''FPLAPW + GGA + SO'' was similar to the previous one (''FPLAPW + GGA''), but now a full relativistic correction, considering the spin-orbit coupling [23] was applied.

The fourth set, named ''FPLAPW + GGA(NR)'' goes in the opposite direction, by avoiding relativistic corrections. This is done in order to investigate whether such corrections really affect the results.

Finally, the fifth set of calculations, named ''VASP(GGA)'', was performed using the Projector Augmented Wave (PAW) [24] method as implemented into the ''VASP'' code [5] using the same GGA approximation [22] and scalar relativistic corrections as in the second set.

The equilibrium lattice constants at the ground state have been determined through the calculation of the minimum value of the total energy. As the total energy is the important parameter in the present approach, particular care was taken when performing convergence tests. Following the

WIEN2k notation, the convergence of the order of 10^{-6} Ry in the total energy has been achieved by using suitable values of RK_{max}, ℓ_{max} and number of k-points, which are control parameters for the convergence in the FP-LAPW calculation. The convergence can be achieved by different paths and here we have chosen to first vary RK_{max}, keeping ℓ_{max} and number of k-points fixed, then vary ℓ_{max} (keeping RK_{max} and number of k-points fixed) and, last vary the number of k-points, with the other parameters fixed. The self-consistent process has been done until the difference of total energies per unit cell was smaller than 10^{-6} Ry in two subsequent calculations. In the case of the VASP code calculations the electronic wave-functions of the PAW [24] method, with a kinetic energy cutoff of 370 eV in a plane-wave basis set expansion was used. We notice that the Fe potential is the one which requires the highest cutoff energy and the 370 eV value used here is 30% above the largest VASP code default value for Fe(268 eV) and 40% above the largest VASP code default value for Mo (225 eV). Using 370 eV assures that we are in a very converged (less than 1 meV) alloy cutoff energy region, a convergence criterion which had already roughly been achieved even using the largest default value for Fe (268 eV). However,we notice that the use of the minimum (201 eV) Fe VASP code default cuttof energy value should not be used, since the total energy differs by some tenths of eV from the converged 370 eV value. All calculations were performed spin polarized and convergence in total energy was achieved when it differed by less than 1.0×10^{-5} eV between two self-consistent iterations,for a given cut-off energy value. The integration in the Brillouin zone was sampled employing a $15 \times 15 \times 15$ k-point mesh in the Monkhorst–Pack scheme [25]. The electronic energy levels were broadened using the Methfessel–Paxton Scheme [26] with a broadening of 0.1 eV.

The calculated total energies for compound Φ (with $\Phi = $ B2, B32, or $D0_3$) with Mo_xFe_y stoichiometry (and $n = x + y$ atoms in the unity formula) are denoted by $U^{\Phi}_{Mo_xFe_y}$, and must be converted into formation energies, $\Delta^f U^{\Phi}_{Mo_xFe_y}$, per mol of atoms in the reference state of the mechanical mixture of the components (with BCC structure) for implementation in the CVM. This is done using

$$\Delta^f U^{\Phi}_{Mo_xFe_y} = \frac{U^{\Phi}_{Mo_xFe_y} - xU^{A2}_{Mo} - yU^{A2}_{Fe}}{n}. \quad (1)$$

As the A2 structure of iron is known to be ferromagnetic, all calculations where spin polarized. The calculated formation energies correspond, therefore, to magnetically ordered compounds in some of the cases.

The formation energies of the four compounds are used as input parameters in the statistical mechanics formalism (CVM) adopted for the calculation of the phase diagram. The CVM was first proposed by Kikuchi [14] as a method to derive entropy expressions for arbitrary lattices in arbitrary approximations. Later it was recognized that the CVM furnishes a standard procedure to derive factorable partition functions of lattice systems within the mean-field approach [18].

The central concept of the CVM is the "basic cluster", which corresponds to a geometric figure contained in the reference lattice (not necessarily restricted to lattice points, see Ref. [27]) which represents the range of correlation lengths explicitly considered in the approximation. In the present work, the IT cluster approximation for the BCC lattice has been employed (Fig. 1). The CVM formalism in the IT cluster approximation has been thoroughly outlined in several previous publications by the present group [15, 16, 28] and therefore only the aspects which are relevant to the discussion of the results will be reproduced here.

The internal energy (U) of a BCC lattice with N sites (containing 6N irregular tetrahedra) is written as [29]

$$U = 6N \sum_{i,j,k,l=\mathrm{Fe,Mo}} \varepsilon^{\alpha\beta\gamma\delta}_{i,j,k,l} \rho^{\alpha\beta\gamma\delta}_{i,j,k,l}. \quad (2)$$

In this expression, $\rho^{\alpha\beta\gamma\delta}_{i,j,k,l}$ represents the probability of finding an $\{\alpha\beta\gamma\delta\}$ IT cluster with configuration $\{ijkl\}$ (i.e. species i occupying cluster position α, j in cluster position β and so on...) among the 6N tetrahedra of the system and $\varepsilon^{\alpha\beta\gamma\delta}_{i,j,k,l}$ represents the eigenenergy associated with this configuration. The stoichiometric compounds at the ground state correspond to particular configurations: a B2 MoFe stoichiometric compound with N lattice points, for example, may be built by $6N$ tetrahedra with configuration FeFe-MoMo, while the B32 MoFe, $D0_3$ Mo_3Fe, and $MoFe_3$ stoichiometric compounds are similarly obtained using the MoFeMoFe, MoMoMoFe, and MoFeFeFe configurations. Equation (2) may be now applied to these particular cases and the compound formation energies are associated with the corresponding cluster eigenenergies. In the case of the B2 MoFe compound, for example:

$$\varepsilon^{\alpha\beta\gamma\delta}_{\mathrm{Mo,Mo,Fe,Fe}} = \frac{\Delta^f U^{B2}_{MoFe}}{6N}. \quad (3)$$

It has to be reminded that the eigenenergy matrix $\{\varepsilon^{\alpha\beta\gamma\delta}_{i,j,k,l}\}$ is highly degenerate due to symmetry constraints imposed by the crystal lattice. Both configurations FeMoFeMo and MoFeMoFe, for example, represent a B32 MoFe stoichiometric compound, differing only by a translation

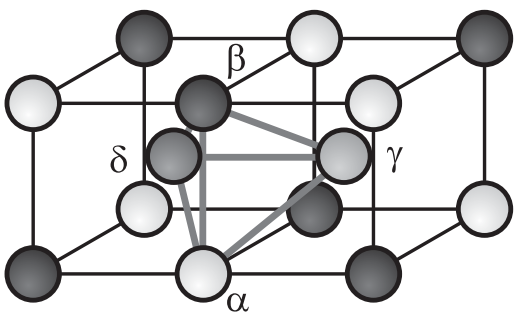

Figure 1 The irregular tetrahedron (IT) cluster in the BCC lattice.

of the origin of the lattice by the vector $(a_0/2)[111]$ (where a_0 represents the lattice constant of the B32 structure). Since the energy of a compound cannot depend on the choice of the origin, it follows that $\varepsilon^{\alpha\beta\gamma\delta}_{\mathrm{Mo,Fe,Mo,Fe}} = \varepsilon^{\alpha\beta\gamma\delta}_{\mathrm{Fe,Mo,Fe,Mo}}$. The same is true for the two remaining degenerate configurations FeMoMoFe and MoFeFeMo.

Set $\{\varepsilon^{\alpha\beta\gamma\delta}_{i,j,k,l}\}$, including the two reference values, $\varepsilon^{\alpha\beta\gamma\delta}_{\mathrm{Mo,Mo,Mo,Mo}} = \varepsilon^{\alpha\beta\gamma\delta}_{\mathrm{Fe,Fe,Fe,Fe}} = 0$, contains all information needed for the description of the system. It is a common practice in the literature, however, to further decompose the configuration eigenenergies into pair contributions (nearest and next-nearest neighbors), completing the set with other cluster interactions (see, e.g. Refs. [29, 30]). This will not be done in the present work, since the results are better appreciated using the compound formation energies instead.

2.1 Cluster variation method calculation With the definition of the internal energy, Eq. (2), we may build the free energy, F, of the system as:

$$F = U - TS + \sum_{i,j,k,l=\mathrm{Fe,Mo}} \frac{\mu^*_i + \mu^*_j + \mu^*_k + \mu^*_l}{4} \rho^{\alpha\beta\gamma\delta}_{i,j,k,l}. \quad (4)$$

In this expression, S stands for the configurational entropy of a BCC lattice in the IT cluster approximation, which is found, e.g. in Ref. [31]. Variables μ^*_m represent the chemical potential of component m in the "barycentric" reference state, defined by transformation

$$\mu^*_{\mathrm{Mo}} = \frac{\mu_{\mathrm{Mo}} - \mu_{\mathrm{Fe}}}{2} = -\mu^*_{\mathrm{Fe}}, \quad (5)$$

where μ_{Mo} and μ_{Fe} are the chemical potentials of molybdenum and iron in any reference state (e.g. the Standard Element Reference, SER [32]).

Using the identity

$$U - TS = N \sum_{i=\mathrm{Mo,Fe}} \mu_i x_i \quad (6)$$

and substituting it, with (5), into (4), we obtain

$$F = N\left(\frac{\mu_{\mathrm{Mo}} + \mu_{\mathrm{Fe}}}{2}\right). \quad (7)$$

Equation (4) is minimized via a dedicated algorithm called "Natural Iteration Method", NIM [33]. For given values of T and $\{\mu^*_{\mathrm{Mo}}\}$ one may eventually obtain different solutions for the minimum (either global or local) of F[1] using suitable choices of initial conditions. Supposing the algorithm converges to different phases (say, λ and ϕ), the equilibrium condition will be given by

$$F^{\lambda} = F^{\phi}. \quad (8)$$

[1] In the present calculations, the convergence condition was set to a difference smaller than $10^{-4}\, k_{\mathrm{B}} \cdot \mathrm{K}$ between two values of F obtained in subsequent iterations of the NIM ($1\, k_{\mathrm{B}} \cdot \mathrm{K} = 8.3145\, \mathrm{J\,mol^{-1}}$).

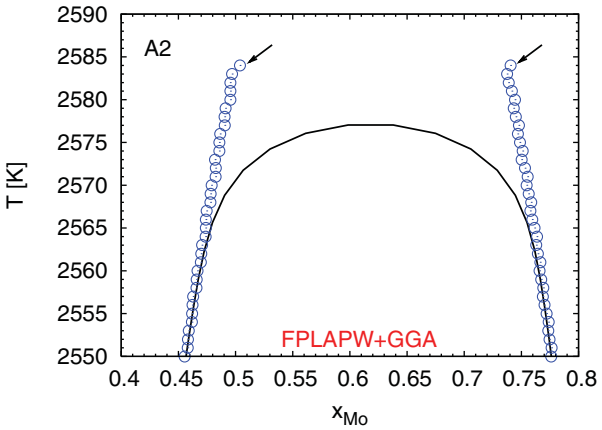

Figure 2 (online color at: www.pss-b.com) Detail of the dome corresponding to the FPLAPW + GGA case close to its maximum, illustrating the procedure used in the calculation. The arrows indicate the composition of the A2 phases in the equilibrium corresponding to the first converged point.

A phase diagram calculation corresponds to mapping all possible solutions of Eq. (8) as functions of T and μ^*_{Mo}, for all pairs of stable configurations, λ and ϕ.

In systems containing miscibility gaps the different solutions correspond to phases with identical symmetry and different compositions. Close to the maximum of the gap the difference in composition vanishes, so obtaining the solution of Eq. (8) is troublesome in this region. All calculations here reported were performed using a temperature step of 1 K close to the maximum of the gap, always starting from the first converged point, corresponding to the highest temperature, proceeding downwards in the temperature scale. This first converged point is determined by trial-and-error and is included in the plot. In order to avoid breaking points in this area, all calculated points corresponding to a given miscibility gap were sorted by increasing x_{Mo} and the curve was drawn using a Bezier smoothing algorithm[2]. In all cases here reported, it was verified that the drawn miscibility gap obtained using this procedure has a maximum temperature which is about 5–10 K smaller than the last converged point in the calculation. Figure 2 shows the detail close to the maximum of the dome for the "FPLAPW + GGA" calculation as an example to illustrate the limitations of this procedure. In this figure, the symbols represent the outcome of the calculation and the continuous line corresponds to the drawn curve. The arrows indicate the composition of the A2 phases obtained in the first converged point.

In estimating the error involved in this procedure, two considerations must be made. First, the way the NIM algorithm converges to the conodal boundary is such that the compositions of both phases move at each iteration towards the center of the phase diagram. Close to the critical point (i.e. the maximum of the miscibility gap) the algorithm presents an increasing inertia and, hence, these converged

[2] Using the Gnuplot v. 4.4 software.

points are subject to a systematic error which tends to widen the gap. This systematic error decreases as the temperature decreases, both because the lower inertia and due to the increasing distinction between the two solutions. Second, the CVM is a member of the "mean-field" class of solutions to statistical mechanics problems and these solutions are known to be unable to deal with the diverging correlation length close to the critical point [34]. This leads to a systematic error which tends to move the miscibility gap maximum towards higher temperatures. Away from the critical point, however, the "mean-field" solutions are known to be reliable [34], hence the procedure adopted in the present work, probably, results in a better estimate of the true solution to the model.

3 Results and discussion In Table 1, we present the results obtained in the electronic structure calculations. This table lists the total energies,equilibrium lattice parameters, a_0, and average magnetic moments, μ, of the six compounds forming the basis of the cluster expansion for the BCC Mo–Fe system using the different approximations described in Section 2. We note that total energies vary a lot among the different approaches, especially between WIEN2k and VASP, but only their difference is relevant, what is expressed by the compound formation energies, to be described latter on in this work. The WIEN2k code control parameters for the electronic structure calculations were not very sensitive to the choice of the methodological set. The condition $RK_{\max} = \ell_{\max}$ was obtained in the convergence of all compounds (in all sets), which was reached with $RK_{\max} = 10$, 10, where the radii $R = 2.0$ a.u. for all atomic species were used, and 413 k-points. The maximum energy ($E_{\max}$) of the energy window in the "FPLAPW + GGA + SO" calculation was increased to 10 Ry and an additional $p_{1/2}$ radial wave function was added in this case.

Concerning equilibrium lattice parameters and magnetic momenta, we observe that the largest variations are observed between the LSDA set and the others, which used the GGA approximation. This effect is already reported in the literature (see Ref. [1] and references therein). It must be kept in mind that only the pure elements can be experimentally observed. The experimental values for equilibrium

Table 1 Total energies, $U^{\Phi}_{\mathrm{Mo}_x\mathrm{Fe}_y}$, calculated for the six compounds forming the basis for the cluster expansion applied to the BCC Mo–Fe system using the five sets of assumptions described in the text.

calculation	stoichiometry	structure	a_0	μ	B (GPa)	$U^{\Phi}_{\mathrm{Mo}_x\mathrm{Fe}_y}$
FPLAPW + LSDA	Fe	A2	0.276	2.03	247	−2541.1693
	Mo	A2	0.312	0	291	−8090.8711
	MoFe	B2	0.295	1.58	268	−10632.0151
	MoFe	B32	0.592	1.76	261	−21264.0340
	$MoFe_3$	$D0_3$	0.570	1.90	267	−15714.3683
	Mo_3Fe	$D0_3$	0.608	1.76	273	−26813.7394
FPLAPW + GGA	Fe	A2	0.284	2.22	181	−2545.6126
	Mo	A2	0.316	0	260	−8099.1827
	MoFe	B2	0.301	2.03	217	−10644.7702
	MoFe	B32	0.603	2.08	215	−21289.5413
	$MoFe_3$	$D0_3$	0.584	2.22	198	−15736.0045
	Mo_3Fe	$D0_3$	0.618	2.17	232	−26843.1187
FPLAPW + GGA + SO	Fe	A2	0.284	2.24	178	−2545.6144
	Mo	A2	0.316	0	247	−8099.2073
	MoFe	B2	0.301	2.03	225	−10644.7965
	MoFe	B32	0.603	2.08	211	−21289.5936
	$MoFe_3$	$D0_3$	0.584	2.21	198	−15736.0344
	Mo_3Fe	$D0_3$	0.618	2.17	235	−26843.1938
FPLAPW + GGA(NR)	Fe	A2	0.286	2.31	170	−2527.2640
	Mo	A2	0.318	0	242	−7954.6888
	MoFe	B2	0.303	2.09	197	−10481.9275
	MoFe	B32	0.607	2.13	196	−20963.8584
	$MoFe_3$	$D0_3$	0.583	2.20	180	−15536.4606
	Mo_3Fe	$D0_3$	0.617	2.11	214	−26391.2899
VASP(GGA)	Fe	A2	0.284	2.21	176	−0.6110
	Mo	A2	0.315	0	268	−0.8045
	MoFe	B2	0.300	1.98	217	−1.3886
	MoFe	B32	0.601	2.02	216	−2.7825
	$MoFe_3$	$D0_3$	0.583	1.93	200	−2.6197
	Mo_3Fe	$D0_3$	0.617	2.03	235	−2.9835

The values of average magnetic moment in the unit cell, μ, are also presented (in Bohr magnetons, μ_B). Equilibrium lattice parameters are expressed in nm and energy values are represented in Rydberg (1 Ry = $2.1798741 \times 10^{-18}$ J).

lattice parameter at room temperature are 0.28670 nm for A2 Fe and 0.31470 nm for A2 Mo [35], which agree remarkably well with the values reported in Table 1 for those sets which used the GGA approximation. The same is true for the reported value of equilibrium average magnetic moment of A2 Fe ($\mu = 2.216\,\mu_B$) [36].

Concerning the bulk modulus, experimental values for both Fe and Mo can be obtained either by using polycrystal data (respectively 169.8 and 261.2 GPa) or by using single crystal elastic constants (respectively 167 and 265 GPa) [35]. As expected, the calculated values for Mo are in better agreement in the cases where both relativistic corrections and GGA are used. The comparisons for Fe show a slightly better agreement in the case of the VASP calculation, but it should be reminded that the calculated values refer to the ground state ($T = 0$ K), while experimental data are usually taken at room temperature, and that elastic constants usually show small decrescent dependencies with increasing temperature [37, 38].

Table 2 shows the calculated formation energies of all compounds in the reference state of the mechanical mixture of BCC Mo (A2 Mo) and BCC Fe (A2 Fe) in the five sets of calculations.

The results of Table 2 are shown graphically in Fig. 3. This form of presentation was chosen in order to allow a better visualization of the differences between each set.

Figure 3 shows that some of the qualitative features of the formation energies for these compounds do not depend on the calculation set. For instance, all formation energies are positive and also the stability sequence is the same in all cases: B2-MoFe and B32-MoFe have the largest (i.e more positive) values of formation energy, while the formation energy of the $D0_3$-Mo_3Fe compound, in spite of being smaller than both B2 and B32, is larger than the formation energy of the $D0_3$-$MoFe_3$. Figure 3, however, shows that variations of the order of ± 1 kJ mol^{-1} in the formation energy of a given compound are observed for all compounds depending on the basic assumptions used in the electronic structure calculations. Curiously this "accuracy" is of the same order of magnitude as the smallest estimated error in standard calorimetric techniques [39].

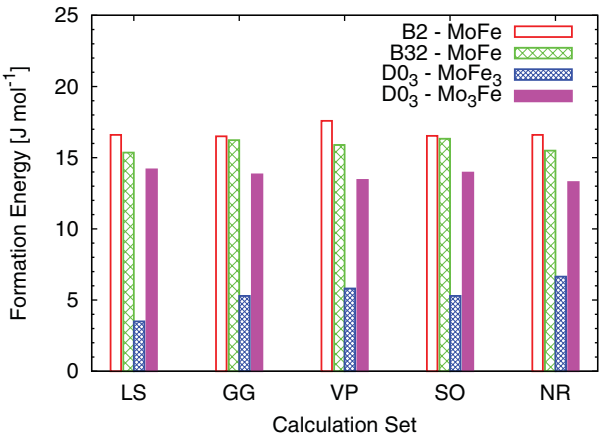

Figure 3 (online color at: www.pss-b.com) Formation energies of the compounds used to build the basis for the cluster expansion of the Mo–Fe system according to the five sets of assumptions described in the text: LS = FPLAPW + LSDA, GG = FPLAPW + GGA, SO = FPLAPW + GGA + SO, NR = FPLAPW + GGA(NR) and VP = VASP(GGA).

Table 2 Formation energies of the compounds in the five calculation sets (kJ mol^{-1}).

Calculation	stoichiometry	structure	$\Delta^f U^{\Phi}_{Mo_xFe_y}$
FPLAPW + LSDA	MoFe	B2	+16.60
	Mo_3Fe	$D0_3$	+14.18
	MoFe	B32	+15.36
	$MoFe_3$	$D0_3$	+3.50
FPLAPW + GGA	MoFe	B2	+16.50
	Mo_3Fe	$D0_3$	+13.83
	MoFe	B32	+16.23
	$MoFe_3$	$D0_3$	+5.29
FPLAPW + GGA + SO	MoFe	B2	+16.53
	Mo_3Fe	$D0_3$	+13.95
	MoFe	B32	+16.33
	$MoFe_3$	$D0_3$	+5.29
FPLAPW + GGA(NR)	MoFe	B2	+16.60
	Mo_3Fe	$D0_3$	+13.29
	MoFe	B32	+15.50
	$MoFe_3$	$D0_3$	+6.65
VASP(GGA)	MoFe	B2	+17.59
	Mo_3Fe	$D0_3$	+13.44
	MoFe	B32	+15.89
	$MoFe_3$	$D0_3$	+5.81

Figure 4 shows the corresponding phase diagrams. We see that all versions show the same qualitative features: an asymmetric miscibility gap, skewed towards Mo-rich alloys. At a closer inspection, however, quantitative differences become evident. The first converged point, for example, ranges from 2474 K (FPLAPW + GGA(NR)) to 2602 K (FPLAPW + LSDA), and its position ranges from $x_{Mo} \sim 0.61$ to 0.64 at% Mo, depending on the set. The shape of the miscibility gap is also affected by the assumptions used in the electronic structure calculation, and all phase diagrams should be considered distinct in this aspect. The phase diagrams also show what seems to be a dramatic change in curvature close to the maximum; analysis of Fig. 2 shows that this effect is an illusion caused by the adopted scale.

Figure 5 shows in detail the iron-rich side of the five phase diagrams plotted jointly for a better appreciation of the differences between the calculation sets. This figure shows, for example, that choosing the temperature of a hypothetical heat treatment for solubilization of Mo-rich particles in the iron matrix would lead to a difference of about 200 K depending on the approximation used for the electronic structure calculation at this composition range. This equilibrium is not observed in the experimental phase diagram

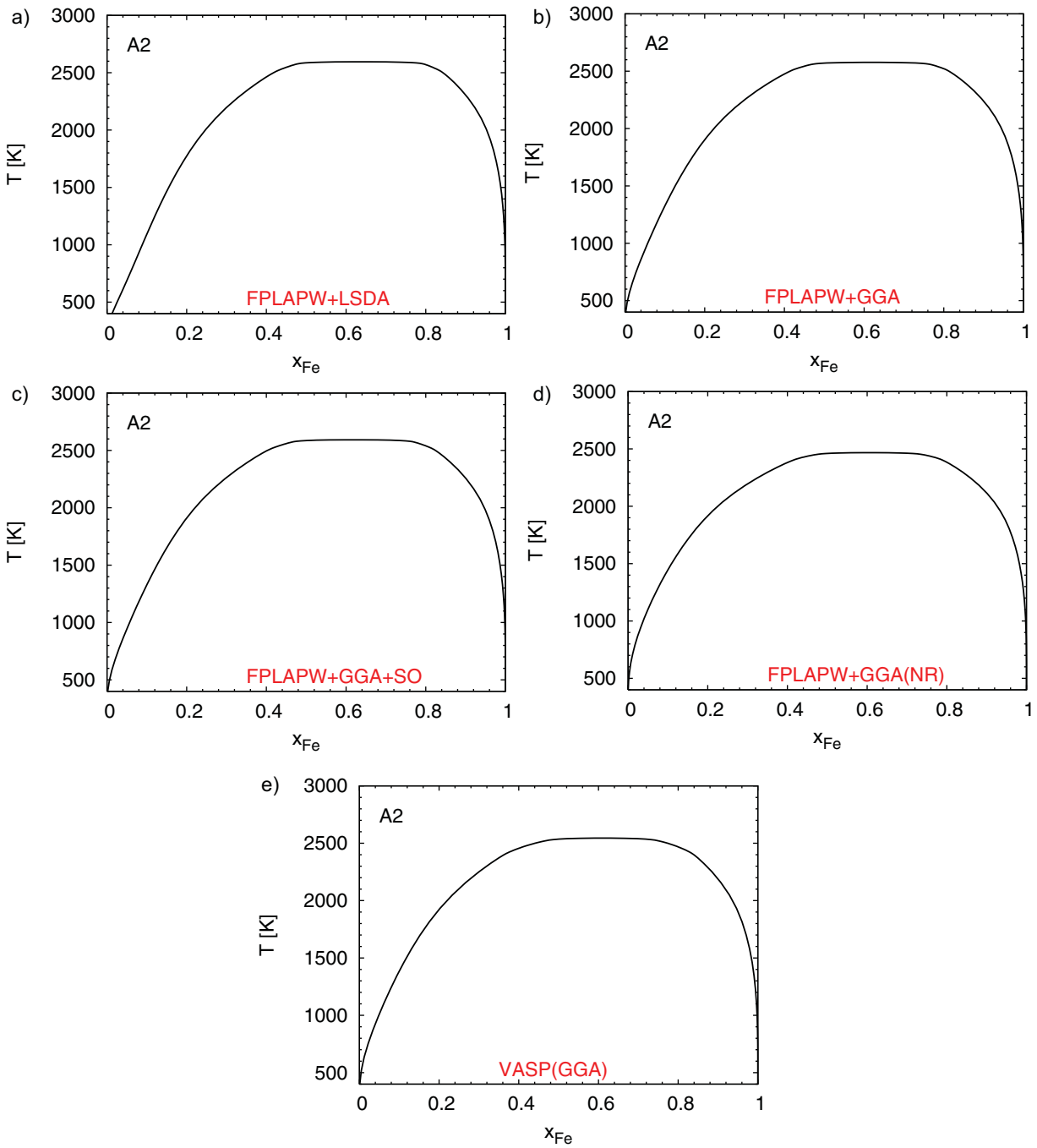

Figure 4 (online color at: www.pss-b.com) The BCC Mo–Fe phase diagrams calculated using the basic assumptions described in the text: (a) FPLAPW + LSDA case, (b) FPLAPW + GGA case, (c) FPLAPW + GGA + SO case, (d) FPLAPW + GGA(NR) case, and (e) VASP(GGA) case.

due to the stability of other intermetallic compounds, which are not directly related to the BCC lattice. For instance the Laves ($MoFe_2$), the μ and the R phases are found in equilibrium with the A2 Fe phase [40, 41]. These intermetallic phases, however, are characterized by restricted homogeneity ranges and complex crystal structures, and hence, these equilibria are highly dependent on the thermodynamic model of the iron-rich BCC solid solution. It can be concluded, therefore, that they would be characterized by a similar uncertainty[3] as the one observed here.

[3] A direct calculation of these equilibria using the existing thermodynamic models for the Laves, μ and R phases [40] is not feasible due to the overestimation of the temperature scale in the *ab initio* calculation, which should be corrected prior any attempt of comparison with experimental results.

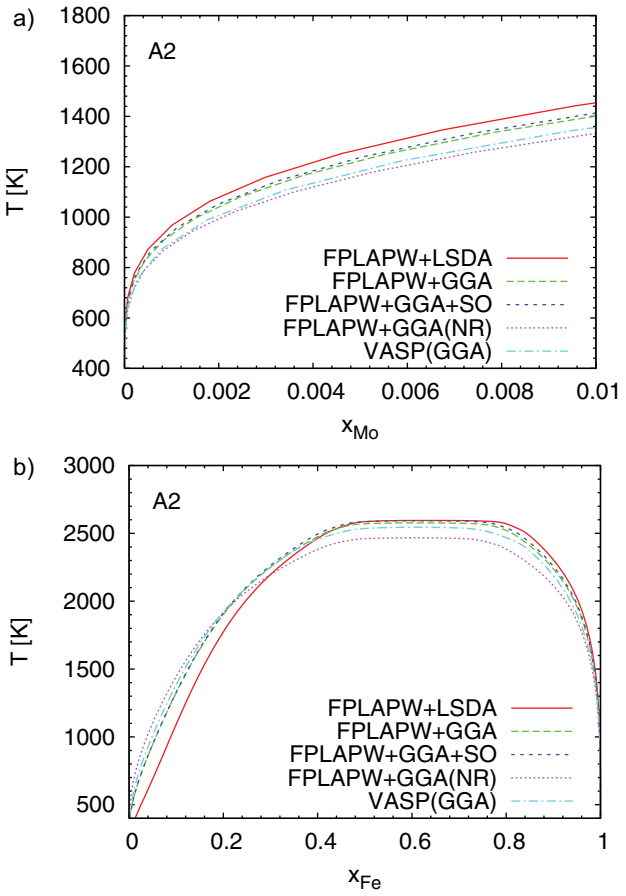

Figure 5 (online color at: www.pss-b.com) (a) Detail of the iron-rich side of the BCC Mo–Fe phase diagrams using the five calculation sets described in the text. (b) Superposition of the five phase diagram cases.

The results reported here clearly demonstrate that the basic assumptions used for the electronic structure calculations have a small, but significative, impact on the calculation of *ab initio* phase diagrams. It must be reminded that this is not a simple question of improving an approximation. For example, the GGA is very often considered to be a better approximation compared with the LSDA, since it is able to correctly predict the ground state of ferromagnetic iron to be BCC [42], but there are cases (e.g. when non-bonded interactions dominate) where the LSDA results give a better agreement with measurements.

The choice between FPLAPW in the WIEN2k code and PAW in the VASP code is also basically motivated by efficiency on the electronic structure calculation. This is true even for the case of the relativistic corrections, where a clear sequence of improvement in the approximations can be identified. For some cases they may lead to insignificant changes in the calculated phase diagram (as in the present case), justifying the use of a simpler approximation, but other systems may need an improved approximation. In particular, the use of mixed approximations in the calculation of a phase diagram can lead to uncontrolled variations of the formation energies of the compounds.

Finally, as pointed out here, no unique BCC Mo–Fe *ab initio* phase diagram can be defined, at least in the current stand of the technique. As a consequence, *ab initio* calculations point at a sort of average phase diagram, reliable concerning the qualitative features, but with quantitative variations inherent also from the basic assumptions used in the electronic structure calculations.

4 Conclusion The metastable BCC Mo–Fe phase diagram has been calculated using the cluster expansion method by combining electronic structure calculations using five different basic assumptions and the CVM in the IT approximation.

In all cases, the resulting phase diagrams show the same qualitative feature (an asymmetric miscibility gap, skewed towards Mo-rich alloys), but with quantitative differences concerning both its extent in the temperature scale and its shape. To our knowledge, this is the first example of an investigation that compares phase diagrams that were calculated with DFT codes which base their electronic structure calculations on different basic assumptions. We have shown that there are small but significant differences in certain calculated phase diagram features such as limited solubilities on the flanks of a miscibility gap.

We have shown that particular care in the choice of the basic assumptions for the calculation has to be taken when a precise determination of details, as the corners of the phase diagram are aimed. As it is already known, these must be unique (and clearly defined) in the course of a given calculation. Our results also shows that the choice of the exchange and correlation functional is important and, not so much expected for these (not so heavy) intermetallic d-compounds, the inclusion of relativistic effects can change the determination of fine details of *ab initio* phase diagrams.

The calculated values of compound formation energies using different sets of assumptions for the electronic structure calculations agree qualitatively, but show quantitative variations of about $\pm 1\,\mathrm{kJ\,mol^{-1}}$ between the sets, which can be assumed as an estimate of accuracy of this measurement. Curiously the same accuracy is expected in standard calorimetric methods in a "best case" scenario.

Acknowledgements This work has been financially supported by the São Paulo State Research Funding Agency (FAPESP, São Paulo-SP, Brazil), by the Brazilian National Research Council (CNPq, Brasília-DF, Brazil), and by the Coordenação de Aperfeiçoamento de Pessoal de Nível Superior (CAPES, Brasília-DF, Brasil), and used some facilities at LCCA-USP and CENAPAD-UNICAMP, Brazil and at UNAC-FCNM-CI, Peru. We want to thank Prof. Robert Laskowski for very important discussions.

References

[1] K. Capelle, Bras. J. Phys. **36**, 1318 (2006).
[2] D. Nguyen-Manh, A. M. Bratkovsky, D. G. Pettifor, A. R. C. Westwood, K. S. Kumar, and R. W. Cahn, Phil. Trans. R. Soc. Lond. A 351 **529**, (1995).
[3] P. Blaha, K. Schwarz, G. K. H. Madsen, D. Kvasnicka, and J. Luitz, WIEN2K, An augmented Plane Waves + Local Orbitals Program for Calculating Crystal Properties (Karlheinz Schwarz, Tech. Universität Wien, Austria, 2001), ISBN 3950103112.
[4] P. E. Blöchl, Phys. Rev. B **50**, 17953 (1994).
[5] G. Kresse and J. Furthmüller, Comp. Mater. Sci. **6**, 15 (1996).
[6] L. A. Errico, M. Rentería, and H. M. Petrilli, Physica B: Condens. Matter **389**, 37 (2007).
[7] L. A. Terrazos, H. M. Petrilli, M. Marszalek, H. Saitovitch, P. R. J. Silva, P. Blaha, and K. Schwarz, Solid State Commun. **121**, 525 (2002).
[8] P. Wodniecki, A. Kulinska, B. Wodniecka, S. Cottenier, H. M. Petrilli, M. Uhrmacher, and K. P. Lieb, Europhys. Lett. **77**, 43001 (2007).
[9] L. A. Errico, M. Rentería, and H. M. Petrilli, Phys. Rev. B **75**, 155209 (2007).
[10] A. Kulinska, P. Wodniecki, B. Wodniecka, H. M. Petrilli, L. A. Terrazos, M. Uhrmacher, and K. P. Lieb, J. Phys.: Condens. Matter **21**, 095405 (2009).
[11] H. M. Petrilli and S. Frota-Pessoa, Phys. Rev. B **44**, 10493 (1991).
[12] P. Blaha, K. Schwarz, and P. H. Dederichs, Phys. Rev. B **37**, 2792 (1988).
[13] A. van de Walle and G. Ceder, J. Phase Equilibr. **23**, 348 (2002).
[14] R. Kikuchi, Phys. Rev. **81**, 988 (1951).
[15] P. G. Gonzales-Ormeño, H. M. Petrilli, and C. G. Schön, Scripta Mater. **53**, 751 (2005).
[16] P. G. Gonzales-Ormeño, H. M. Petrilli, and C. G. Schön, Scripta Mater. **54**, 1271 (2006).
[17] N. Sodré, P. G. Gonzales-Ormeño, H. M. Petrilli, and C. G. Schön, Calphad **33**, 576 (2009).
[18] D. De Fontaine, Solid State Phys. **43**, 33 (1994).
[19] V. Blum and A. Zunger, Phys. Rev. B **69**, 020103(R) (2004).
[20] J. P. Perdew and Y. Wang, Phys. Rev. B **45**, 13244 (1992).
[21] D. D. Koelling and B. N. Harmon, J. Phys. C **10**, 3107 (1977).
[22] J. P. Perdew, K. Burke, and M. Ernzerhof, Phys. Rev. Lett. **77**, 3865 (1996).
[23] A. H. MacDonald, W. E. Pickett, and D. D. Koelling, J. Phys. C **13**, 2675 (1980).
[24] G. Kresse and D. Joubert, Phys. Rev. B **59**, 1758 (1999).
[25] H. J. Monkhorst and J. D. Pack, Phys. Rev. B **13**, 5188 (1976).
[26] M. Methfessel and A. T. Paxton, Phys. Rev. B **40**, 3616 (1989).
[27] R. Kikuchi, Progr. Theor. Phys. Suppl. **115**, 1 (1994).
[28] P. G. Gonzales-Ormeño and C. G. Schön, J. Alloys Compd. **470**, 301 (2008).
[29] C. G. Schön and G. Inden, J. Chim. Phys. PCB **94**, 1143 (1997).
[30] R. McCormack, D. de Fontaine, C. Wolverton, and G. Ceder, Phys. Rev. B **51**, 15808 (1995).
[31] L. T. F. Eleno and C. G. Schön, CALPHAD **27**, 335 (2003).
[32] K. Hack, The SGTE Casebook: Thermodynamics at Work (The Institute of Materials, London, 1996).
[33] R. Kikuchi, J. Chem. Phys. **60**, 1071 (1974).
[34] K. Huang, Statistical Mechanics (Wiley-VCH, New York, 1987,).
[35] W. F. Gale and T. C. Totenmeier, Smithels Metals Reference Handbook, 8th ed. (Elsevier, Amsterdam, 2004).
[36] T. B. Massalski (ed.), Binary Alloy Phase Diagrams, Vol. 1, 2nd ed. (ASM International, Metals Park-OH, 1990),
[37] J. A. Rayne and B. S. Chandrasekhar, Phys. Rev. **122**, 1714 (1961).
[38] J. M. Dickinson and P. E. Armstrong, J. Appl. Phys. **38**, 602 (1967).
[39] R. Ferro, G. Borzone, G. Cacciamani, and R. Raggio, Thermochim. Acta **347**, 103 (2000).
[40] J. Andersson, Calphad **12**, 9 (1988).
[41] J. Houserová, J. Vřešťál, and M. Šob, Calphad **29**, 133 (2005).
[42] P. Bagno, O. Jepssen, and O. Gunnarsson, Phys. Rev. B **40**, 1997 (1989).